HHS Public Access

Author manuscript

J Mol Cell Cardiol. Author manuscript; available in PMC 2020 July 01.

Published in final edited form as:

J Mol Cell Cardiol. 2019 July ; 132: 24–35. doi:10.1016/j.yjmcc.2019.05.004.

Electrophysiologic and Molecular Mechanisms of a Frameshift *NPPA* Mutation Linked with Familial Atrial Fibrillation

Ambili Menon, PhD[a], **Liang Hong, MD, PhD**[a], **Eleonora Savio-Galimberti, MD, PhD**[b], **Arvind Sridhar, MS**[a], **Seock-Won Youn, PhD**[a,c], **Meihong Zhang, PhD**[a], **Kaylen Kor, BE**[d], **Marcia Blair, BS**[d], **Sabina Kupershmidt, PhD**[e], and **Dawood Darbar, MD**[a,c,f]

[a]Departments of Medicine, University of Illinois at Chicago, Chicago, IL

[b]Department of Biomedical Sciences, Philadelphia College of Osteopathic Medicine, Philadelphia, PA

[c]Physiology and Biophysics, University of Illinois at Chicago, Chicago, IL

[d]Department of Pharmacology, Vanderbilt University Medical Center

[e]Department of Nursing, University of South Dakota Sioux Falls, SD

[f]Pharmacology, University of Illinois at Chicago, Chicago, IL

Abstract

A frameshift (fs) mutation in the natriuretic peptide precursor A (*NPPA*) gene, encoding a mutant atrial natriuretic peptide (Mut-ANP), has been linked with familial atrial fibrillation (AF) but the underlying mechanisms by which the mutation causes AF remain unclear. We engineered 2 transgenic (TG) mouse lines expressing the wild-type (WT)-*NPPA* gene (*H-WT-NPPA*) and the human fs-Mut-*NPPA* gene (*H-fsMut-NPPA*) to test the hypothesis that mice overexpressing the human *NPPA* mutation are more susceptible to AF and elucidate the underlying electrophysiologic and molecular mechanisms. Transthoracic echocardiography and surface electrocardiography (ECG) were performed in *H-fsMut-NPPA, H-WT-NPPA*, and Non-TG mice. Invasive electrophysiology, immunohistochemistry, Western blotting and patch clamping of membrane potentials were performed. To examine the role of the Mut-ANP in ion channel remodeling, we measured plasma cyclic guanosine monophosphate (cGMP) and cyclic adenosine monophosphate (cAMP) levels and protein kinase A (PKA) activity in the 3 groups of mice. In *H-fsMut-NPPA* mice mean arterial pressure (MAP) was reduced when compared to *H-WT-NPPA* and Non-TG mice. Furthermore, injection of synthetic *fs-Mut-ANP* lowered the MAP in *H-WT-NPPA* and Non-TG mice while synthetic WT-ANP had no effect on MAP in the 3 groups of mice. ECG characterization revealed significantly prolonged QRS duration in *H-fsMut-NPPA* mice when compared to the other two groups. Trans-esophageal (TE) atrial pacing of *H-fsMut-NPPA* mice

Corresponding Author Contact Information: Dawood Darbar, MBChB, MD, Division of Cardiology, 840 S. Wood St., 920S (MC 715), University of Illinois at Chicago Chicago, IL 60612, Telephone: +1-312-413-8870, Fax: +1-312-413-2948, darbar@uic.edu.

Disclosures: None

showed increased AF burden and AF episodes when compared with *H-WT-NPPA* or Non-TG mice. The cardiac Na^+ (NaV1.5) and Ca^{2+} (CaV1.2/CaV1.3) channel expression and currents (I_{Na}, I_{CaL}) and action potential durations ($APD_{90}/APD_{50}/APD_{20}$) were significantly reduced in *H-fsMut-NPPA* mice while the rectifier K^+ channel current (I_{Ks}) was markedly increased when compared to the other 2 groups of mice. In addition, plasma cGMP levels were only increased in *H-fsMut-NPPA* mice with a corresponding reduction in plasma cAMP levels and PKA activity. In summary, we showed that mice overexpressing an AF-linked *NPPA* mutation are more prone to develop AF and this risk is mediated in part by remodeling of the cardiac Na^+, Ca^{2+} and K^+ channels creating an electrophysiologic substrate for reentrant AF.

Subject Terms:

atrial fibrillation; *NPPA*; frameshift mutation; transgenic mouse models; APD; mechanisms

Keywords

atrial fibrillation; cardiac sodium and calcium channel; *NPPA* frameshift mutation

INTRODUCTION

Atrial fibrillation (AF) is the most common sustained cardiac arrhythmia affecting over 3 million adults in the U.S. at an estimated cost of over 26 million dollars per day [1]. With the aging of the population, the projected number of people with AF is estimated to be 12 million by 2050 [2]. The AF epidemic is further complicated by the lack of effective therapies. Despite recent advances in catheter-based therapies, antiarrhythmic drugs (AAD) continue to be commonly used to treat patients with symptomatic AF [3]. However, response in an individual patient is highly variable and carries risks of proarrhythmia and extra-cardiac toxicity. The limited efficacy of AADs is in part due to the poor understanding of the pathophysiology of AF and failure to target therapy to the underlying mechanisms [4]. One approach to unraveling the molecular pathogenesis of AF is by the identification of key molecules and signaling pathways involved in familial (early-onset) forms of the arrhythmia.

Over the last 15 years, linkage analyses and candidate gene approaches have identified mutations in cardiac ion channels, signaling molecules, and structural proteins linked with familial AF [4]. *KCNQ1*, encoding the cardiac delayed rectifier K^+ channel current (I_{Ks}), was the first gene that segregated with familial AF [5]. Gain-of-function mutations in repolarizing K^+ currents shorten action potential duration (APD) and refractoriness creating a substrate for reentrant AF. In contrast, gain-of-function mutations in depolarizing Na^+ or Ca^{2+} increase APD and refractoriness and increase susceptibility to a triggered mechanism of AF [4]. Ion channel mutations also predispose to AF by triggering early afterdepolarizations (EADs) and prolonging atrial action potential duration (APD). A third mechanism of AF involves modulating expression of gap junction proteins important for cell-to-cell communication with mutations in *GJA5*, encoding connexin-40, associated with familial AF [6].

In 2008, Hodgson-Zingman and colleagues reported a novel frameshift (fs) mutation in the natriuretic peptide precursor A (*NPPA*) gene in a large family of European descent where familial AF segregated as an autosomal dominant trait [7]. The 2 base-pair deletion abolished the normal stop codon resulting in 12 amino acid extension of atrial natriuretic peptide (ANP). Circulating levels of the mutant (Mut)-ANP were 5-10 fold higher in affected family members when compared with wild-type (WT)-ANP, in part, due to resistance to proteolytic degradation of the mutant peptide [8]. While an isolated rat heart model showed that the Mut-ANP shortened the monophasic APD and created a reentrant substrate for AF, the specific ion channels modulated and the underlying molecular mechanisms by which the *NPPA* mutation caused AF are poorly understood. To test the hypothesis that mice overexpressing the human mutant *NPPA* are more susceptible to AF and elucidate the underlying electrophysiologic and molecular mechanisms, 2 transgenic (TG) mouse lines, one expressing the WT-*NPPA* gene (*H-WT-NPPA*), and the other overexpressing the human fs-Mut-*NPPA* gene (*H-fsMut-NPPA*) were engineered.

METHODS

Generation of TG mouse lines:

All breeding and experiments were performed in accordance with protocols approved by the institutional animal care and use committee (IACUC) at the University of Illinois at Chicago (UIC) and Vanderbilt University Medical Center as per NIH guidelines. A triple FLAG-tag (FLAG) DYKDHDGDYKDHDIDYKDDDDK was fused in-frame with the 3' end of either the H-WT-ANP cDNA as well as in H-fsMut-ANP containing the COOH-terminal 12 amino acid extension isolated from the individuals with familial AF (RITAREDKQGWA-DYKDHDGDYKDHDIDYKDDDDK). Thus, both H-WT-NPPA as well as H-fsMut-NPPA TG mice have 22 extra amino acids. The sequence of the triple FLAG tag is: DYKDHDGDYKDHDIDYKDDDDK-stop. WT and mutant FLAG-tagged NPPA sequences were generated using PCR-based methods incorporating restriction enzyme sites, and inserted into the Sal I site of a vector containing the α-myosin heavy chain (MHC) promoter (GenBank Accession #U71441.1). Digestion with EcilI was used to differentiate between H-WT-NPPA and H-fsMut-NPPA.

The DNA was injected directly into the pronuclei of fertilized B6D2 oocytes. TG founders were identified by PCR using a set of primers for the α-MHC promoter and FLAG sequences to verify the insertion/presence of the transgenes in the *H-WT-NPPA* and *H-fsMut-NPPA* mice. TG founder mice were bred with B6D2 mice (Jackson Laboratories, Bar Harbor, ME) and housed in a specific pathogen-free/viral antibody-free animal facility at UIC. Mice used for the experiments were 16-28 weeks of ages. Tail biopsies from the TG mice were isolated to genotype using the following set of primers:

1. NPPA human ORF_F [5'-ACAAGTGCTCAGTGAGCCGAATGAA-3']
2. NPPA human ORF_R [5'-CCCGCCCGAGGGCACCTCCATCTCTCTGGGC-3']
3. Alpha MYHC_F [5'-AAAAGAGGCAGGGAAGTGGT-3']
4. HGH_R [5'-ACTTGCCCCTTGCTCCATAC-3']

PCR analysis with forward and reverse primers in the α-MHC promoter and HGH sequence, respectively, was used to verify the insertion/presence of the transgenes in the mouse strains. We used PCR to confirm the expression of the transgenes using primers that crossed exon-exon boundaries. Automated sequencing to confirm the presence of the SNP, double deletion amino acid and 36 bp extension in the *H-fsMut-NPPA* of the TG mice.

1. Sequencing the DNA of the *H-fsMut-NPPA* Mouse Line: Sequencing of *H-fsMut-NPPA*-Flag PCR fragments confirmed the presence of the genetic variant, the double deletion amino acid and the 36-bp extension.

2. Determination of Number of Copies of *H-NPPA* Gene Inserted in the Mouse DNA from the 2 TG Lines Generated: Quantitative real time PCR (qRT-PCR) was used to determine the number of copies of NPPA for each TG mouse line using the 2(−ΔΔC(T) Method [9, 10]. Human control genomic DNA (known to have 2 *NPPA* copies) was used as the calibrator, with *β*-actin as the housekeeping gene.

3. Cardiac Tissue and Plasma Concentration of Human ANP in TG mouse lines: We used an ANP-Competitive ELISA Kit (Thermo Fischer Scientific, Waltham, MA) to measure the circulating levels of H-ANP in the plasma as per the manufacture's instruction. Blood samples from the 3 groups of mice were collected through cardiac puncture and centrifuged immediately and isolated plasma samples were stored in EDTA containing vials at −80°C until assayed. For cardiac tissue concentration we used an immunoassay H-ANP α (1-28) EIA Kit, Phoenix Pharmaceuticals, Burlingame, CA). We performed peptide extraction on the atrial cardiac tissue isolated from the 3 groups of mice as per manufacturer's instruction. The extracted peptides from the mice were then diluted with 1x Assay buffer and used for the immunoassay. It is important to note that the 2 assays detected both the WT-ANP which consists of 28 amino acids and the Mut-ANP containing an additional 12 amino acids.

4. Invasive Electrophysiology: Mice were anesthetized with 1-2% isoflurane in 95% O_2. Trans-esophageal (TE) pacing was performed using a 1.1F octapolar catheter (CIBer Cath; NuMED, Hopkinton, NY) inserted into the esophagus to the level of the heart. Adequate catheter positioning was confirmed by TE pacing performed at 800 μV. ECG channels were amplified (0.1 mV/cm) and filtered between 0.05 and 400 Hz [11]. A computer-based data acquisition system (Emka Technologies) was used to record a 3-lead body surface ECG, and 4 intraesophageal bipolar electrograms. TE pacing was performed using 2-msec current pulses delivered by an external stimulator (STG3008-FA, Multichannel Systems, Reutlingen, Germany). Standard clinical EP pacing protocols were used to induce AF as previously described [12, 13]. Briefly, atrial burst pacing was performed with 300 cycles of 2 msec bursts at 800 mV and at a cycle length (CL) of 50 msec, 40 msec, 30 msec, 25 msec, 20 msec and 15 msec. Next, Verheule's pacing protocol was performed utilizing 2 sec burst cycles at CL of 40 msec, and then decreasing in each successive burst with a 2 msec decrement down to a CL of 20 msec [12]. This was followed by TE atrial burst pacing with eight 50 ms and four 30 ms CL train episodes repeated several times, up to a maximum 1 min time limit of total stimulation. The series of bursts were repeated twice. AF was

defined as a period of rapid irregular atrial rhythm lasting at least 5 seconds. If one or more bursts in the 2 series of bursts evoked an AF episode, AF was considered to be inducible in that animal; otherwise, AF was considered to be non-inducible.

5. Blood Pressure (BP) Measurements: BP was recorded in conscious mice using a noninvasive tail cuff BP System (CODA, Kent Scientific, Torrington, CT). Mice were placed into restraint tubes over a warming plate, and the BP tail cuff was attached. After a period of acclimation, a total of 30 cycles per animal was decided on to optimize the number of measurements as previously described [14, 15]. The first 10 cycles were not used in the final analysis. The remaining 20 cycles were evaluated according to the manufacturer's recommendations. Mean arterial pressure (MAP) was recorded in a proper environment (room temperature, lighting, and noise-free atmosphere) for the 3 groups of mice with 12 animals in each group.

The synthetic peptide used in the BP measurements was the full length H-fs-Mut-ANP consisting of 40 amino acids: [NH2]SLRRSSCFGGRMDRIGAQSGLGCNSFRYRITAREDKQGWA-[COOH]. This was synthesized, purified to 96% by high-performance liquid chromatography, and verified by peptide sequencing and mass spectroscopy (Thermo-Fischer Scientific, Waltham, MA). This peptide was injected (intraperitoneal, IP) at a physiological concentration (16 pmol/kg) to the 3 groups of mice and MAP was re-measured 30 mins and 120 mins post injection. The above experiment was repeated using synthetic WT-ANP peptide [NH2] SLRRSSCFGGRMDRIGAQSGLGCNSFRY-[COOH] consisting of 28 amino acids. This peptide was also injected at the same physiological concentration as described above.

6. Western blot: Atrial lysates were prepared from flash frozen hearts. Lysates were prepared from Non-TG, *H-WT-NPPA* and *H-fsMut-NPPA* mice and were size fractionated on 8-10% SDS polyacrylamide gels. The resolved gels were electro transferred on nitrocellulose membrane. Membranes were probed with anti-FLAG rabbit polyclonal antibody (#ab1170, Abcam, USA), anti-NaV1.5 rabbit polyclonal antibody (#ASC005, Almone, Israel), anti-CaV1.2 and anti-CaV1.3 polyclonal antibodies (#PA5-77297 and #PA5-77299, Invitrogen Thermo-Fischer Scientific, USA) at 4°C overnight. The gels were developed using anti-rabbit HRP (1:2500 dilution, Abcam, USA) and scanned on Biorad Gel Doc (Hercules, USA). Protein signal densities were normalized to the corresponding Actin signal densities and used for plotting data.

7. Isolation of Mouse Atrial Myocytes: The procedure for isolating mouse atrial myocytes has been described previously [16]. Briefly summarizing, mice were administered a 0.2 ml intraperitoneal injection of heparin (1000 IU/ml) to prevent blood clotting. Mice were anaesthetized using isoflurane inhalation and then the heart was excised into Tyrode's solution (35°C) consisting of (in Mm)140 NaCl, 5.4 KCl, 1.2 KH_2PO_4, 1.0 $MgCl_2$, 1.8 $CaCl_2$, 5.55 glucose and 5 Hepes, with pH adjusted to 7.4 with NaOH. The right and the left atrial appendage was dissected from the heart and cut into strips and then equilibrated and washed in 'low Ca^{2+}, Mg^{2+} free solution containing 140 NaCl, 5.4 KCl, 1.2 KH_2PO_4, 0.2 $CaCl_2$, 50 taurine, 18.5 glucose, 5 Hepes and 1 mg ml–1 bovine serum albumin (BSA), with pH adjusted to 6.9 with NaOH. Atrial tissue strips were digested in 5 ml of 'low Ca^{2+}/Mg^{2+}-

free' solution containing collagenase (type II; Worthington Biochemical Corporation), elastase (Worthington Biochemical Corporation, Lakewood, NJ, USA) and protease (type XIV; Sigma Chemical Company, St. Louis, MO, USA) for 30 min. Then the tissue was transferred to 5ml of modified KB solution containing: 100 potassium glutamate, 10 potassium aspartate, 25 KCl, 10 KH_2PO_4, 2 $MgSO_4$, 20 taurine, 5 creatine, 0.5 EGTA, 20 glucose, 5 Hepes and 0.1% bovine serum albumin, with pH adjusted to 7.2 with KOH. The tissue was mechanically agitated using a wide bore pipette. This procedure yielded individual atrial myocytes with cellular automaticity that was recovered after readapting the cells to a physiological concentration of Ca^{2+}.

8. AP Recording in Mouse Atrial Cells: Both left and right atrial myocytes were isolated as described previously [22]. Atrial cells were studied in current-clamp mode by injecting stimulus current (1-2 nA, 2 msec) at 1 Hz. APs were recorded at 37°C in Tyrodes solution containing: 140 NaCl, 5.4 KCl, 1 $MgCl_2$, 1.8 $CaCl_2$, 5.5 glucose, 10 HEPES (pH adjusted to 7.4 with NaOH). The pipette solution contained: 125 K-glutamate, 20 KCl, 10 NaCl, 5 EGTA, 10 HEPES (pH adjusted to 7.2 with KOH).

9. Na^+ (I_{Na}), Ca^{2+} (I_{CaL}) and K^+ (I_{Ks}) Current Recordings in Mouse Atrial Cells: Atrial myocytes from both the atria were isolated from all the 3 groups of mice using a protocol described previously [22] for viable cardiac myocytes isolation from adult mouse hearts. Voltage-clamp measurements were performed in whole-cell configurations using an Axopatch 200B amplifier controlled by pClamp10 software [23]. For Na^+ current (I_{Na}) recording, the external solution contained: 5 NaCl, 130 CsCl, 1 $CaCl_2$, 1 $MgCl_2$, 10 glucose, 20 HEPES, and 10μM nifedipine (pH adjusted to 7.3 with CsOH). An intracellular solution contained: 5 NaCl, 135 CsF, 10 EGTA, 5 MgATP, 10 HEPES, with pH adjusted to 7.2 with CsOH. Steady-state activation G-V for I_{Na} were fitted by the Boltzmann equation as previously described [24-25]: $G/Gmax=1/(1+exp(V-V1/2)/K$ where G/Gmax is the relative conductance normalized by the maximal conductance, V1/2 is the potential of half activation, V is test, and k was the Boltzmann coefficient. Pipettes had 2-4 MΩ access resistance. Current densities were calculated by whole-cell current amplitude and capacitance value taken from readings of the amplifier after electronic subtraction of the capacitive transients.

For calcium current (*ICa-L*) recordings, the external solution contained 150 Tris, 10 glucose, 1 $MgCl_2$, and 10 $CaCl_2$, adjusted to pH 7.4 with methanesulfonic acid. An intracellular solution contained 135 CsCl, 10 EGTA, 1 $MgCl_2$, 4 Mg-ATP, and 10 HEPES adjusted to pH 7.3 with CsOH. *ICa-L* are activated by depolarization to +10mV from a holding potential of −80mV

For I_{Ks} recording, the external solution contained: 140 NaCl, 4 KCl, 1.8 $CaCl_2$, 1.2 $MgCl_2$, 10 glucose, 10 HEPES, supplemented with 10 μM nifedipine, adjusted to pH 7.4 with NaOH. I_{Ks} recordings were obtained as 100 μM chromanol 293B-sensitive current. An intracellular solution contained: 100 potassium aspartate, 20 KCl, 2 $MgCl_2$, 5 Mg-ATP, 5 EGTA, 10 HEPES, and adjusted to 7.2 with KOH. I_{Ks} currents were elicited by using 4 s voltage-clamp steps to test potentials of −30 to +50 mV, with 20 mV increments.

10. Assessment of PKA Activation in Atrial Tissue: To determine PKA activation we used an ELISA-based PKA kinase activity assay kit (Ab139435, Abcam, Cambridge, UK). This kit was used for measuring the PKA activity in the lysates of frozen atrial cardiac tissue. The frozen heart powders were mixed with the lysis buffer containing: 20 MOPS, 50 β-glycerol phosphate, 5 EGTA, 2 EDTA, 1% NP40, complete protease inhibitor cocktail (Roche Diagnostics, West Sussex, UK) and phosphatase inhibitor cocktail 3 (Sigma, Gillingham, UK). The samples were centrifuged at 2000 χ g for 5 min at 4°C to remove the cell debris. Protein concentration was adjusted to 4 mg/ml using BCA protein assay. About 1 μg of protein of each sample were assayed according to the manufacturer's instructions.

11. Plasma cAMP and cGMP Measurements: In-vitro assays (cGMP EIA kit, Cayman Chemical Company Inc.) were performed as per manufactures instructions. The cAMP complete enzyme immunoassay kit from Assay Designs was used as directed by the manufacturer (#ab65355, Abcam, Cambridge, UK). Blood samples from cardiac puncture were centrifuged immediately after collection, and isolated plasma was stored in EDTA-containing vials at −80°C until assayed.

12. Statistical Analysis: Data are presented as mean ± standard error of the mean (SEM) or mean ± standard deviation (SD) as indicated. For datasets with normal distributions, statistical significance was determined by Student's t-test (two-tailed) for two groups or analysis of variance (ANOVA) as appropriate.

RESULTS

H-fsMut-NPPA and *H-WT-NPPA* TG mice express FLAG-tagged ANP in the 4 cardiac chambers and *H-fsMut-NPPA* mice show elevated ANP levels:

We generated 2 TG mouse models that overexpress the human-*NPPA* gene. The protein expression of FLAG-ANP was confirmed by Western blot analysis by targeting the FLAG-epitope (Figure 1A). DNA sequencing confirmed the presence of the variant (T>C), double deletion of amino acid and the addition of 36-bp to the original sequence (Figure 1B). Copy number of h-NPPA expressed in each one of the transgenic lines determined by qRT-PCR showed H-fsMut-NPPA line expresses 3.3±1.9 copies of h-NPPA (mean ± SD, n=3 mice), which suggest that this line overexpresses NPPA. The h-WT-NPPA (n=3 mice) expresses a similar number of copies (2) than human controls (n=5 human blood samples). In both cases, H-NPPA is expressed in addition to the expression of the endogenous mouse Nppa (Nppa-m).

Biological activity of H-ANP-FLAG tag:

cGMP values in cells exposed to ANP were normalized to baseline levels measured in untreated cells and expressed as fold increase. Exposure of HL-1 cells to WT-ANP increased cGMP production (1.9±0.8 fold; n=6 cells). This increase in cGMP was similar to the increase observed when the cells were exposed to WT-ANP-FLAG (1.8±0.5 fold, n=6 cells; Supplementary Figure 1). These findings strongly suggest that the FLAG-tag has no biological activity.

Intracardiac and plasma concentrations of H-ANP levels were higher in *H-fsMut-NPPA* mice as compared to *H-WT-NPPA* mice. Intracardiac tissue concentration of H-α-ANP in *H-fsMut-NPPA* mice (72.23±3.80 pg/ml, P<0.0001, n=12) was ~2.6-fold higher than in *WT-NPPA* mice (27.17±2.147 pg/ml, n=12; Figure 1C). The plasma level of H-α-ANP in *H-fsMut-NPPA* mice (30.71 ±0.81 pg/ml, P<0.0001, n=12) was ~3-fold higher than in *H-WT-NPPA* mice (10.31 ±0.70 pg/ml, n=12; Figure 1D) mice.

H-fsMut-NPPA mice have lower BP compared to *H-WT-NPPA* and Non-TG mice:

ANP is known to act as a cardiac hormone that regulates blood volume and BP. Studies have shown that defects in the ANP pathway contribute to major diseases such as hypertension, cardiac hypertrophy and heart failure (HF) [17-19]. To assess the role of WT-ANP and Mut-ANP on the BP in *H-WT-NPPA* and *H-fsMut-NPPA* mice we used the non-invasive tail cuff BP method. The MAP was lowest in *H-fsMut-NPPA* (76±4 mmHg, n=12) as compared to *H-WT-NPPA* (102±3 mmHg, n=12) and Non-TG (121 ±2 mmHg, n=12) mice (Table 1). To ensure the effect was indeed due to H-Mut-ANP, we injected the 3 groups of mice with a synthetic fsMut-ANP at a physiological concentration (16 pmol/kg) and then re-measured the MAP. Synthetic fsMut-ANP reduced the MAP in *H-fsMut-NPPA* (52±3 mmHg, P<0.0001, n=12), *H-WT-NPPA* (80±2 mmHg, P0.0001, n=12) and Non-TG (107±3 mmHg, P<0.0001, n=12). Importantly, 120 min post-injection the MAP in the 3 groups of mice returned to baseline levels. We repeated the experiment with synthetic WT-ANP at a physiological concentration (16 pmol/kg). Measurement of the MAP 30 mins post injection revealed no change in the MAP in all 3 groups of mice (Table 1B). This data suggests that the elevated levels of Mut-ANP seen in *H-fsMut-NPPA* mice leads to reduced MAP observed in these mice.

Electrocardiogram (ECG) and echocardiographic characterization of *H-fsMut-NPPA* mice:

ECG characterization revealed significantly prolonged QRS duration in *H-fsMut-NPPA* mice when compared to *H-WT-NPPA* and Non-TG mice (Table 2 **and** Supplementary Figure 2A). In contrast, the PR interval (Table 2) and P-wave duration (Non-TG: 15.7±2.6 sec, *H-WT-NPPA*: 16.8 ±4.3 sec; and *H-fsMut-NPPA*: 18.3±3.9 sec) were unchanged in Non-TG, *H-WT-NPPA* and *H-fsMut-NPPA* mice. TTE showed no significant differences in left ventricular (LV) function and left atrial (LA) diameter across the 3 groups of mice (n=6 mice/group; Supplementary Table 1 and Figure 2B). Thus atrial size and ventricular function were preserved in the 3 groups of mice.

H-fsMut-NPPA mice are more prone to AF:

As the *NPPA* mutation in humans segregates with AF [7], we tested the hypothesis that *H-fsMut-NPPA* mice are more susceptible to AF as compared with *H-WT-NPPA* and Non-TG mice. To evaluate the arrhythmogenic phenotype of the 3 groups, we performed TE programmed stimulation of the atria which is commonly used to experimentally induce AF in mice [20]. Upon atrial stimulation (Figure 2A) *H-fsMut-NPPA* mice showed increased AF burden per mouse (176±56 sec, n=11; Figure 2B) as compared to *H-WT*-NPPA (20±8.4 sec, n=10) and Non-TG mice (0 sec, n=8) and increased number of AF episodes per mouse (6.18±3.4; AF inducibility) versus *H-WT-NPPA* mice (1.8±1.9) and Non-TG mice (0; Figure

2C). *H-fsMut-NPPA* mice demonstrated AF incidence of 100% versus 50% in *H-WT-NPPA* and 0% in Non-TG mice (Figure 2D). Thus, *H-fsMut-NPPA* mice had more readily inducible AF and a greater total burden of AF in each mouse.

Atrial fibrosis in *H-fsMut-NPPA* mice:

Atrial interstitial fibrosis has been implicated in conduction abnormalities that result in an increase in AF vulnerability [21]. To investigate whether the increased inducibility of AF in *H-fsMut-NPPA* mice is due to structural remodeling, atrial tissue from *H-fsMut-NPPA, H-WT-NPPA* and Non-TG mice (n=5) was stained with Masson's trichrome (Supplementary Figure 3). There was no evidence of atrial fibrosis in both TG mouse models.

Shortening of the APD_{90} is observed in *H-fsMut-NPPA* mice:

Electrical remodeling of the atria is considered as one of the substrate essential for AF [22, 23]. To investigate the role of APD in increased AF burden in *H-fsMut-NPPA* mice, we conducted patch-clamp studies to measure atrial APD at 90% repolarization (APD_{90}), and the maximum upstroke of the AP in atrial myocytes isolated from the 3 groups of mice. Representative APs for the 3 groups of mice are shown in Figure 3A. The maximum upstroke velocity was reduced in *H-fsMut-NPPA* mice as compared to *H-WT-NPPA* mice (138.2 ± 4.57 mV/ms vs 159.7 ± 6.707 mV/ms, $P<0.05$; n=6 mice/group; Figure 3B). APD_{90} was significantly reduced in *H-fsMut-NPPA* mice versus *H-WT-NPPA* mice (17.63 ± 0.57 ms vs 20.73 ± 0.45, $P<0.01$ n=6 mice/group; Figure 3C). APD_{20} and APD_{50} were also reduced in *H-fsMut-NPPA* mice (2.05 ± 0.14 ms and 5.97 ± 0.38 ms respectively; n=6) when compared to *H-WT-NPPA* (2.78 ± 0.12 ms and 7.22 ± 0.34 ms respectively, n=6) and Non-TG (2.76 ± 0.1 ms and 7.16 ± 0.26 ms respectively, n=6; Figure 3D-E). The resting membrane potential (RMP) and maximum AP amplitude (APA_{max}) were also measured in the 3 groups of mice (Supplementary Figure 4A-B). Thus, *H-fs-Mut-NPPA* mice demonstrated reduced APD_{90}, APD_{50} and APD_{20} and decreased maximum upstroke velocity.

Downregulation of NaV1.5 and I_{Na} in *H-fsMut NPPA* mice with AF:

To explore the underlying electrophysiological mechanisms, protein levels of key ion channels were measured in atrial tissue. In humans, only some *SCN5A* variants are associated with alterations in cardiac repolarization, reduction of APD, and increased susceptibility to AF [24]. Given this association, we sought to determine the role of NaV1.5 expression in *H-fsMut-NPPA* AF phenotype. Western blot of NaV1.5 in Non-TG, *H-WT-NPPA* and *H-fsMut-NPPA* mouse atria revealed a significant reduction in NaV1.5 protein expression in *H-fsMut-NPPA* and *H-WT-NPPA* mice as compared to Non-TG mice (Figure 4A-B). Representative I_{Na} recordings and relative cell conductance are displayed in (Figure 4C-D). Statistical analysis of the normalized I-V plot of I_{Na} density from the 3 groups of mice showed a significant difference between Non-TG vs *H-fsMut-NPPA* ($P<0.0001$) as well as *H-WT-NPPA vs H-fsMut-NPPA* ($P<0.0001$) by 1-way repeated measures ANOVA with Tukey post hoc test (n=6 atrial myocytes/group). The reduction in NaV1.5 expression was reflected in reduced peak I_{Na} density in *H-fsMut-NPPA* mice versus *H-WT-NPPA* and Non-TG (Figure 4E). Our data showed that there were no significant alterations in $V_{1/2}$

among 3 groups of mice suggesting that *H-WT-NPPA* and *H-fsMut-NPPA* did not alter the gating process of the cardiac Na^+ channel (Figure 4F-G).

Reduced CaV1.2 and CaV1.3 expression and $I_{Ca,L}$:

Several studies have reported that the electrophysiological remodeling accompanying episodes of AF could be prevented by pretreatment with Ca^{2+} channel blockers, suggesting that Ca^{2+} overload might initiate changes in gene expression that eventually lead to a downregulation of atrial Ca^{2+} current densities which may be a critical factor in electrophysiological remodeling [24-26]. To further evaluate the electrophysiologic mechanism for the observed shortening of the APD_{90} in *H-fsMut-NPPA* mice, we examined protein expression and density of the voltage-dependent $I_{Ca,L}$. CaV1.2 and CaV1.3 expressions were significantly reduced in *H-fsMut-NPPA* mice as compared with *H-WT-NPPA* and Non-TG mice (Figure 5A-C). We also showed that $I_{Ca,L}$ is markedly reduced in *H-fsMut-NPPA* mice as compared with the other 2 groups of mice (Figure 5D-H). In addition, statistical analysis of normalized I-V plot of $I_{Ca,L}$ density from the 3 groups of mice showed a significant difference between Non-TG vs *H-fsMut-NPPA* mice ($P<0.0001$) and *H-WT-NPPA vs H-fsMut-NPPA* mice ($P<0.05$) by 1-way repeated measures ANOVA with Tukey post hoc test; n=6 atrial myocytes/group (Figure 5E). Furthermore, conductance $V_{1/2}$ was also significantly reduced in *H-fsMut-NPPA* mice as compared with *H-WT-NPPA* mice (Figure 5G).

Increased I_{Ks} current density:

To further elucidate the electrophysiological remodeling we assessed the role of K^+ channels. We showed there was an increase in I_{Ks} in *H-fsMut-NPPA* mice when compared to *H-WT-NPPA* and Non-TG (Figure 6A-C). Thus, shortening of APD in *H-fsMut-NPPA* mice is due to reduced expression of NaV1.5, CaV1.2 and CaV1.3 as well as reduced I_{Na} and $I_{Ca,L}$ and increased I_{Ks} density.

Plasma cGMP and cAMP and PKA activity:

cAMP and cGMP are intracellular second messengers that are intimately involved in humoral physiology of ANP. cGMP regulates cAMP signaling by phosphorylation of distinct downstream targets like PKA and thus regulates its activity [27-30]. To evaluate the role cGMP signaling pathway in cardiac ion channel remodeling in AF, we measured plasma cGMP, cAMP and PKA activity in the 3 groups of mice. Baseline cGMP levels were higher in *H-fsMut-NPPA* (21.70±1.68 pmol/ml, $P<0.0001$, n=12) mice versus *H-WT-NPPA* (7.91±0.75 pmol/ml) and Non-TG mice (4.70±0.62 pmol/ml; Figure 7A). Plasma cAMP level in *H-fsMut-NPPA* mice were markedly reduced (4.26±0.63 pmol/ml, $P<0.0001$, n=12) when compared to the other 2 models (*H-WT-NPPA:* 20.62±0.75 pmol/ml, $P<0.005$; Non-TG: 23.61±1.73 pmol/ml; $P<0.001$; Figure 7B). We also measured PKA activity *in vivo* using the atrial tissue homogenates from the mice. PKA kinase activity was significantly reduced in *H-fsMut-NPPA* mice as compared to *H-WT-NPPA* and Non-TG mice (Figure 7C). This data demonstrates that Mut-ANP modulates the cardiac Na^+ and Ca^{2+} channels by upregulation of cGMP thereby downregulating cAMP levels and PKA kinase activity

DISCUSSION

The first link between a humoral peptide and AF was established when a novel mutation in the gene that encodes ANP was identified in a large Caucasian family [7]. While an isolated rat heart model showed that the Mut-ANP shortened the monophasic APD and likely created a reentrant substrate for AF, the specific ion channels modulated and the underlying molecular mechanism(s) by which the *NPPA* mutation caused AF were unclear. We engineered 2 TG mouse lines expressing *H-fsMut-NPPA* and *H-WT-NPPA* and showed that mice overexpressing the *NPPA* mutation were not only more prone to pacing-induced AF but that this risk is, in part, mediated by remodeling of the cardiac Na^+, Ca^{2+} and K^+ channels creating an electrophysiologic substrate for reentrant AF.

We showed that the *H-fsMut-NPPA* mice overexpressed Mut-ANP (3.3±1.9 copies) as compared with *H-WT-NPPA* and Non-TG mice which expressed 2 copies. However, cumulative evidence supports the elevated cGMP levels are more likely due to reduced degradation of the Mut-ANP rather than differential expression of the 2 peptides. Support for this hypothesis comes from our data showing that Mut-ANP not only elicits electrophysiologic effects including remodeling of cardiac Na^+, Ca^{2+} and K^+ channels but also physiologic effects with marked reduction in MAP when infused in *H-fsMut-NPPA* mice (Table 1). Additional support is provided by a study showing that the WT-ANP and Mut-ANP are not only preferentially degraded by neutral endopeptidase and serine peptidases respectively but that the H-fs-mutation renders ANP resistant to proteolytic degradation [8]. Further, human patients who are heterozygotes for the *NPPA* variant carry only one copy of the mutation [7].

Natriuretic peptides (NPs) with a longer carboxyl terminus have increased resistance to degradation by neutral endopeptidase, in particular, *Dendroaspis augusticeps* natriuretic peptide (DNP), a unique natriuretic peptide isolated from snake venom, which has a carboxyl-terminal extension of 15 amino acids and increased cGMP-stimulating potency [31, 32]. NPs elicit their effects by binding to NP receptors (NPR) including NPR-A, NPR-B, and NPR-C. While NPR-A is activated by ANP, NPR-B is activated by CNP. Furthermore, each receptor is associated with membrane-bound guanylyl cyclase (GC) enzyme that increases the production of cGMP when a peptide is bound. The NPR-C receptor binds to all NPs with similar affinity and activates inhibitory G-proteins (Gi) and reduces intracellular cAMP levels. One study using *NPR-C*$^{-/-}$ knock-out mice showed that ANP affects atrial electrophysiology via NPR-A, whereas the Mut-ANP signals via NPR-C [33]. Furthermore, NPR-C expression is greater in human atria than that of NPR-A. In addition, the same group reported that ANP increases $I_{Ca,L}$ via NPR-A and Mut-ANP decreases $I_{Ca,L}$ via NPR-C. Thus, some of our observed changes in plasma cAMP and PKA activity may in part be linked to changes in adenylyl cyclase/cAMP/PKA activity.

ANP binds to NPR-A, a GC-linked receptor mediating ANP-dependent natriuretic, vasorelaxant and anti-hypertrophic effect [27-29, 34]. The mature 28 amino acid form of ANP is highly conserved across species and hence interaction of H-ANP to mouse NPR-A stimulates cGMP production [30, 35]. In our *H-fsMut-NPPA* mice we observed increased cGMP levels when compared to *H-WT-NPPA* and Non-TG mice along with a corresponding

decrease in cAMP levels and PKA activity. Collectively, these findings support our hypothesis that cGMP activation not only leads to reduced hydrolysis of cAMP but also diminishes PKA activity. Several studies have reported that cAMP and PKA directly modulate NaV1.5 and thereby I_{Na} density [36-39]. Furthermore, increased cGMP is reported to reduce $I_{Ca,L}$ through activation of phosphodiesterase 3 by increasing cAMP hydrolysis [40].

ECG recordings in the 3 groups of mice showed that there was QRS prolongation in the *H-fsMut-NPPA* mice which, in part, reflects downregulation of NaV1.5. A normal LA diameter, atrial volume, LV function and the absence of increased atrial fibrosis in *H-fsMut-NPPA* mice strongly suggests that the increased AF burden observed in our 4-6-month old *H-fsMut-NPPA* mice is not related to atrial structural remodeling. Progressive electrical remodeling of cardiac ion channels is the electrophysiologic hallmark of AF [5, 41]. Previous reports have convincingly showed that natriuretic peptides have potent effects on cardiac electrophysiology [40, 42, 43]. Hua et al [33] showed increased AF inducibility in mouse hearts exposed to Mut-ANP with atrial burst pacing: 62.5% (5/8) of the hearts developed disorganized activation patterns with re-entrant and multiple ectopic foci. Our findings are consistent with this result showing that *H-fsMut-NPPA* mice are more prone to develop AF after atrial burst pacing. Studies have reported that the AP upstroke (dV/dtmax), a major determinant of the conduction velocity in the atria [42], is regulated by the I_{Na} and $I_{Ca,L}$ which are major targets for natriuretic peptides in the atria [33, 40, 42, 43], Several studies have shown that electrical remodeling of the atria characterized by the shortening of APD is due to alteration in the expression and function of L-type Ca^{2+} and inward rectifier K^+ channels [44]. In chronic AF patients, $I_{Ca,L}$ decrease and I_{Ks} increase contribute to the APD shortening [45]. Shortened APD_{90} in atrial cells isolated from *H-fsMut-NPPA* mice in combination with reduced NaV1.5 and CaV1.2/1.3 expression and decreased I_{Na} and $I_{Ca,L}$ densities strongly support ionic remodeling and reduced maximum upstroke velocity creating a reentrant substrate for AF in our *NPPA* mouse model.

Although the precise mechanism(s) by which *NPPA* decreases expression of Na^+ and Ca^{2+} channels remain unclear a number of studies have shown that ANP plays an important role in the expression of voltage-gated ion channels. One study showed that ANP reduced the α-subunit of the epithelial Na^+ channel mRNA expression in mice [46] and the peptide modulates *KCNQ1* expression [47]. Another possible mechanism may relate to direct effects of ANP on cardiac ion channels [48]. While there is tremendous interspecies variation of the effect in part related to varied expression of ANP-interacting receptors and differential protein expression levels of downstream targets, ANP directly modulates Na^+ and Ca^{2+} channels through cGMP signaling pathways [49, 50]. A third mechanism by which *NPPA* may decrease expression of Na^+ and Ca^{2+} channels is by regulating expression of the homeobox transcription factor PITX2, which has been associated with the development of AF. *PITX2* works synergistically with *Nkx2-5* to activate the Nppa promoter [51] and as such regulates remodeling of cardiac ion channels [52]. Thus, modulation of *PITX2* gene expression may be another potential mechanism by which *NPPA* regulates Na^+ and Ca^{2+} channel gene expression.

It is important to note that reduced PKA activity does not necessarily reduce peak I_{Na} and $I_{Ca,L}$ and depends to some extent on which residues are phosphorylated. Na^+ and Ca channels are phosphorylated by specific kinases. Several studies have reported that phosphorylation of NaV1.5 at non-canonical PKA sites in loop I-II, S526 and S529 not only increases NaV1.5 current but also expression [53, 54]. Since commercial antibodies are not available for these sites, we were unable to show a direct correlation between reduced PKA activity and decreased NaV1.5 channel expression and current in *H-fsMut-NPPA* mice. In the absence of PKA stimulation, the greatest density of NaV1.5 channels is in the perinuclear area and activation of PKA promotes trafficking of Na^+ channels to the plasma membrane. These studies suggest that activation of PKA is essential for trafficking of NaV1.5 channels and current [54]. A reduction in $I_{Ca,L}$ is mediated by activation of the cGMP pathway and cGMP stimulation of PDE2 activity causing inhibition of cAMP/PKA pathway [54, 55].

Our study has a number of limitations. The best model in which to study the pathophysiology of the AF-linked *NPPA* mutation is the patient. However, challenges associated with procuring LA tissue, in-vivo imaging of thin-walled atria, and heterogeneity of the underlying substrate render animals an attractive model to study the underlying mechanisms of AF. Furthermore, TG murine models expressing cardiac ion channel mutations and signaling proteins have identified shortening of the APD, creation of a reentry substrate, and generation of early- and delayed afterdepolarization triggered activity associated with ryanodine receptor-2 dysfunction as important mechanisms underlying AF [56-58]. In our *H-fsMut-NPPA* mice we observed increased cGMP levels when compared with H-WT-NPPA and Non-TG mice along with a corresponding decrease in cAMP levels and PKA activity (Figure 7). Although we did not show this directly, several studies have reported that both cAMP and PKA directly modulate NaV1.5 and I_{Na} density [36-39]. Furthermore, increased cGMP reduces $I_{Ca,L}$ through activation of PDE3 by increasing cAMP hydrolysis [40]. Combining existing studies and our findings collectively support the hypothesis that cGMP activation leads to reduced hydrolysis of cAMP and diminishes PKA activity. Demonstrating that upregulating cGMP and downregulating cAMP levels/PKA activity would lead to the same effects would conclusively confirm the role of the cGMP signaling pathway in the pathogenesis of AF in our *H-fsMut-NPPA* mice. Another potential limitation is that we did not measure plasma and cardiac tissue concentrations of the H-Mut-ANP in our *H-fsMut-NPPA* mice as the both the assays we used measured both the H-WT-ANP and H-Mut-ANP. However, we showed that there was a graded increase in both tissue and plasma concentrations of ANP levels across the 3 groups of mice (Figure 1C-D) supporting elevated H-Mut-ANP levels in *H-fsMut-ANP* mice. A more contemporary approach to generating a TG mouse model would use CRISPR to knock-in the mutation. However, this technology was not available when the *NPPA* mouse model was first generated in 2009.

In conclusion, we showed that mice overexpressing an *NPPA* mutation linked with familial AF are more susceptible to pacing-induced AF and this risk is mediated, in part, by remodeling of the cardiac Na^+, Ca^{2+} and K^+ channels creating an electrophysiologic substrate for reentrant AF and modulation of the cGMP signaling pathway.

Supplementary Material

Refer to Web version on PubMed Central for supplementary material.

Acknowledgements:

We thank Dr. Jeffrey Robbins (Cincinnati, OH) for providing us with the α-MHC transgenic vector, and the staff of the Vanderbilt Transgenic Mouse/Embryonic Stem Cell Shared Resource for the blastocyst microinjections. Staining and imaging of histological samples were performed at the VUMC Pathology Service and the VUMC Cell Imaging Shared Resource.

Sources of Funding: American Heart Association (AHA) Established investigator Award (0940116N), NIH R01HL124935 and T32 HL139439 (DD).

Non-standard abbreviations

AF	atrial fibrillation
AAD	antiarrhythmic drug
APD	action potential duration
cGMP	cyclic guanosine monophosphate
fs	frameshift
H-WT-NPPA	humanized wild-type natriuretic precursor peptide A
I_{CaL}	calcium channel current
I_{Na}	sodium channel current
LA	left atrium
Mut-ANP	mutant atrial natriuretic peptide
TE	trans esophageal
TG	transgenic
TTE	transthoracic echocardiogram

References

1. O'Reilly DJ, Hopkins RB, Healey JS, Dorian P, Sauriol L, Tarride JE, et al. The burden of atrial fibrillation on the hospital sector in Canada. Can J Cardiol. 2013;29:229–35. [PubMed: 22652091]
2. Miyasaka Y, Barnes ME, Gersh BJ, Cha SS, Bailey KR, Abhayaratna WP, et al. Secular trends in incidence of atrial fibrillation in Olmsted County, Minnesota, 1980 to 2000, and implications on the projections for future prevalence. Circulation. 2006;114:119–25. [PubMed: 16818816]
3. Duytschaever M, Demolder A, Phlips T, Sarkozy A, El Haddad M, Taghji P, et al. Pulmonary vein isolation with vs. without continued antiarrhythmic drug treatment in subjects with recurrent atrial fibrillation (POWDER AF): results from a multicentre randomized trial. Eur Heart J. 2018;39:1429–37. [PubMed: 29211857]
4. Darbar D, Roden DM. Genetic mechanisms of atrial fibrillation: impact on response to treatment. Nat Rev Cardiol. 2013;10:317–29. [PubMed: 23591267]

5. Chen YH, Xu SJ, Bendahhou S, Wang XL, Wang Y, Xu WY, et al. KCNQ1 gain-of-function mutation in familial atrial fibrillation. Science. 2003;299:251–4. [PubMed: 12522251]
6. Firouzi M, Ramanna H, Kok B, Jongsma HJ, Koeleman BP, Doevendans PA, et al. Association of human connexin40 gene polymorphisms with atrial vulnerability as a risk factor for idiopathic atrial fibrillation. Circ Res. 2004;95:e29–33. [PubMed: 15297374]
7. Hodgson-Zingman DM, Karst ML, Zingman LV, Heublein DM, Darbar D, Herron KJ, et al. Atrial natriuretic peptide frameshift mutation in familial atrial fibrillation. N Engl J Med. 2008;359:158–65. [PubMed: 18614783]
8. Dickey DM, Yoder AR, Potter LR. A familial mutation renders atrial natriuretic Peptide resistant to proteolytic degradation. J Biol Chem. 2009;284:19196–202. [PubMed: 19458086]
9. Livak KJ, Schmittgen TD. Analysis of relative gene expression data using real-time quantitative PCR and the 2(-Delta Delta C(T)) Method. Methods. 2001;25:402–8. [PubMed: 11846609]
10. Pfaffl MW. A new mathematical model for relative quantification in real-time RT-PCR. Nucleic Acids Res. 2001;29:e45. [PubMed: 11328886]
11. van Oort RJ, McCauley MD, Dixit SS, Pereira L, Yang Y, Respress JL, et al. Ryanodine receptor phosphorylation by calcium/calmodulin-dependent protein kinase II promotes life-threatening ventricular arrhythmias in mice with heart failure. Circulation. 2010;122:2669–79. [PubMed: 21098440]
12. Verheule S, Sato T, Everett Tt, Engle SK, Otten D, Rubart-von der Lohe M, et al. Increased vulnerability to atrial fibrillation in transgenic mice with selective atrial fibrosis caused by overexpression of TGF-beta1. Circ Res. 2004;94:1458–65. [PubMed: 15117823]
13. Li N, Wang T, Wang W, Cutler MJ, Wang Q, Voigt N, et al. Inhibition of CaMKII phosphorylation of RyR2 prevents induction of atrial fibrillation in FKBP12.6 knockout mice. Circ Res. 2012;110:465–70. [PubMed: 22158709]
14. Hosoda C, Hiroyama M, Sanbe A, Birumachi J, Kitamura T, Cotecchia S, et al. Blockade of both alpha1A- and alpha1B-adrenergic receptor subtype signaling is required to inhibit neointimal formation in the mouse femoral artery. Am J Physiol Heart Circ Physiol. 2007;293:H514–9. [PubMed: 17384126]
15. Johns C, Gavras I, Handy DE, Salomao A, Gavras H. Models of experimental hypertension in mice. Hypertension. 1996;28:1064–9. [PubMed: 8952597]
16. Ackers-Johnson M, Li PY, Holmes AP, O'Brien SM, Pavlovic D, Foo RS. A simplified, Langendorff-free method for concomitant isolation of viable cardiac myocytes and nonmyocytes from the adult mouse heart. Circ Res. 2016;119:909–20. [PubMed: 27502479]
17. de Bold AJ. Atrial natriuretic factor: a hormone produced by the heart. Science. 1985;230:767–70. [PubMed: 2932797]
18. Koller KJ, Goeddel DV. Molecular biology of the natriuretic peptides and their receptors. Circulation. 1992;86:1081–8. [PubMed: 1327579]
19. Song W, Wang H, Wu Q. Atrial natriuretic peptide in cardiovascular biology and disease (NPPA). Gene. 2015;569:1–6. [PubMed: 26074089]
20. Li N, Wang T, Wang W, Culter MJ, Wang Q, Voigt N, et al. Inhibition of CaMKII phosphorylation of RyR2 prevents induction of atrial fibrillation in FKBP12.6 knockout mice. Circ Res 2012;110:465–70. [PubMed: 22158709]
21. Everett THt, Olgin JE. Atrial fibrosis and the mechanisms of atrial fibrillation. Heart Rhythm. 2007;4:S24–7. [PubMed: 17336879]
22. Dun W, Boyden PA. Aged atria: electrical remodeling conducive to atrial fibrillation. J Interv Card Electrophysiol. 2009;25:9–18. [PubMed: 19280327]
23. Krogh-Madsen T, Abbott GW, Christini DJ. Effects of electrical and structural remodeling on atrial fibrillation maintenance: a simulation study. PLoS Comput Biol. 2012;8:e1002390. [PubMed: 22383869]
24. Yue L, Feng J, Gaspo R, Li GR, Wang Z, Nattel S. Ionic remodeling underlying action potential changes in a canine model of atrial fibrillation. Circ Res. 1997;81:512–25. [PubMed: 9314832]
25. Tieleman RG, De Langen C, Van Gelder IC, de Kam PJ, Grandjean J, Bel KJ, et al. Verapamil reduces tachycardia-induced electrical remodeling of the atria. Circulation. 1997;95:1945–53. [PubMed: 9107184]

26. Daoud EG, Knight BP, Weiss R, Bahu M, Paladino W, Goyal R, et al. Effect of verapamil and procainamide on atrial fibrillation-induced electrical remodeling in humans. Circulation. 1997;96:1542–50. [PubMed: 9315545]
27. Sorbera LA, Morad M. Atrionatriuretic peptide transforms cardiac sodium channels into calcium-conducting channels. Science. 1990;247:969–73. [PubMed: 2154853]
28. Di Benedetto G, Zoccarato A, Lissandron V, Terrin A, Li X, Houslay MD, et al. Protein kinase A type I and type II define distinct intracellular signaling compartments. Circ Res. 2008;103:836–44. [PubMed: 18757829]
29. Vandecasteele G, Verde I, Rucker-Martin C, Donzeau-Gouge P, Fischmeister R. Cyclic GMP regulation of the L-type Ca(2+) channel current in human atrial myocytes. J Physiol. 2001;533:329–40. [PubMed: 11389195]
30. Schoenfeld JR, Sehl P, Quan C, Burnier JP, Lowe DG. Agonist selectivity for three species of natriuretic peptide receptor-A. Mol Pharmacol. 1995;47:172–80. [PubMed: 7838126]
31. Chen HH, Lainchbury JG, Burnett JC Jr. Natriuretic peptide receptors and neutral endopeptidase in mediating the renal actions of a new therapeutic synthetic natriuretic peptide dendroaspis natriuretic peptide. J Am Coll Cardiol. 2002;40:1186–91. [PubMed: 12354448]
32. Johns DG, Ao Z, Heidrich BJ, Hunsberger GE, Graham T, Payne L, et al. Dendroaspis natriuretic peptide binds to the natriuretic peptide clearance receptor. Biochem Biophys Res Commun. 2007;358:145–9. [PubMed: 17475216]
33. Hua R, MacLeod SL, Polina I, Moghtadaei M, Jansen HJ, Bogachev O, et al. Effects of Wild-Type and Mutant Forms of Atrial Natriuretic Peptide on Atrial Electrophysiology and Arrhythmogenesis. Circ Arrhythm Electrophysiol. 2015;8:1240–54. [PubMed: 26227000]
34. Lonardo G, Cerbai E, Casini S, Giunti G, Bonacchi M, Battaglia F, et al. Atrial natriuretic peptide modulates the hyperpolarization-activated current (If) in human atrial myocytes. Cardiovasc Res. 2004;63:528–36. [PubMed: 15276478]
35. Potter LR, Yoder AR, Flora DR, Antos LK, Dickey DM. Natriuretic peptides: their structures, receptors, physiologic functions and therapeutic applications. Handbook of experimental pharmacology. 2009;191:341–66.
36. Le Grand B, Deroubaix E, Couetil JP, Coraboeuf E. Effects of atrionatriuretic factor on Ca2+ current and Cai-independent transient outward K+ current in human atrial cells. Pflugers Arch. 1992;421:486–91. [PubMed: 1281312]
37. Yarbrough TL, Lu T, Lee HC, Shibata EF. Localization of cardiac sodium channels in caveolin-rich membrane domains: regulation of sodium current amplitude. Circ Res. 2002;90:443–9. [PubMed: 11884374]
38. Matsuda JJ, Lee H, Shibata EF. Enhancement of rabbit cardiac sodium channels by beta-adrenergic stimulation. Circ Res. 1992;70:199–207. [PubMed: 1309315]
39. Lee HC, Lu T, Weintraub NL, VanRollins M, Spector AA, Shibata EF. Effects of epoxyeicosatrienoic acids on the cardiac sodium channels in isolated rat ventricular myocytes. J Physiol. 1999;519:153–68. [PubMed: 10432346]
40. Springer J, Azer J, Hua R, Robbins C, Adamczyk A, McBoyle S, et al. The natriuretic peptides BNP and CNP increase heart rate and electrical conduction by stimulating ionic currents in the sinoatrial node and atrial myocardium following activation of guanylyl cyclase-linked natriuretic peptide receptors. J Mol Cell Cardiol. 2012;52:1122–34. [PubMed: 22326431]
41. Nattel S, Dobrev D. Electrophysiological and molecular mechanisms of paroxysmal atrial fibrillation. Nat Rev Cardiol. 2016;13:575–90. [PubMed: 27489190]
42. Azer J, Hua R, Vella K, Rose RA. Natriuretic peptides regulate heart rate and sinoatrial node function by activating multiple natriuretic peptide receptors. J Mol Cell Cardiol. 2012;53:715–24. [PubMed: 22960454]
43. Rose RA, Lomax AE, Giles WR. Inhibition of L-type Ca2+ current by C-type natriuretic peptide in bullfrog atrial myocytes: an NPR-C-mediated effect. Am J Physiol Heart Circ Physiol. 2003;285:H2454–62. [PubMed: 12881210]
44. Voigt N, Heijman J, Wang Q, Chiang DY, Li N, Karck M, et al. Cellular and molecular mechanisms of atrial arrhythmogenesis in patients with paroxysmal atrial fibrillation. Circulation. 2014;129:145–56. [PubMed: 24249718]

45. Caballero R, de la Fuente MG, Gomez R, Barana A, Amoros I, Dolz-Gaiton P, et al. In humans, chronic atrial fibrillation decreases the transient outward current and ultrarapid component of the delayed rectifier current differentially on each atria and increases the slow component of the delayed rectifier current in both. J Am Coll Cardiol. 2010;55:2346–54. [PubMed: 20488306]
46. Luo Y, Xia Q, Xia Z, Tang Y. Atrial natriuretic peptide reduces the alpha-subunit of the epithelial sodium channel mRNA expression in the mouse stria vascularis. Biomed Rep. 2015;3:159–62. [PubMed: 25798240]
47. Zhang J, Zhao Z, Zu C, Hu H, Shen H, Zhang M, et al. Atrial natriuretic peptide modulates the proliferation of human gastric cancer cells via KCNQ1 expression. Oncol Lett. 2013;6:407–14. [PubMed: 24137337]
48. Perrin MJ, Gollob MH. The role of atrial natriuretic peptide in modulating cardiac electrophysiology. Heart Rhythm. 2012;9:610–5. [PubMed: 22083030]
49. Kecskemeti V, Pacher P, Pankucsi C, Nanasi P. Comparative study of cardiac electrophysiological effects of atrial natriuretic peptide. Mol Cell Biochem. 1996;160–161:53–9.
50. Tohse N, Nakaya H, Takeda Y, Kanno M. Cyclic GMP-mediated inhibition of L-type Ca2+ channel activity by human natriuretic peptide in rabbit heart cells. Br J Pharmacol. 1995;114:1076–82. [PubMed: 7540093]
51. Ganga M, Espinoza HM, Cox CJ, Morton L, Hjalt TA, Lee Y, et al. PITX2 isoform-specific regulation of atrial natriuretic factor expression: synergism and repression with Nkx2.5. J Biol Chem. 2003;278:22437–45. [PubMed: 12692125]
52. Chinchilla A, Daimi H, Lozano-Velasco E, Dominguez JN, Caballero R, Delpon E, et al. PITX2 insufficiency leads to atrial electrical and structural remodeling linked to arrhythmogenesis. Circ Cardiovasc Genet. 2011;4:269–79. [PubMed: 21511879]
53. Tateyama M, Rivolta I, Clancy CE, Kass RS. Modulation of cardiac sodium channel gating by protein kinase A can be altered by disease-linked mutation. J Biol Chem. 2003;278:46718–26. [PubMed: 14500710]
54. Zhou J, Yi J, Hu N, George AL Jr., Murray KT. Activation of protein kinase A modulates trafficking of the human cardiac sodium channel in Xenopus oocytes. Circ Res. 2000;87:33–8. [PubMed: 10884369]
55. Weiss S, Oz S, Benmocha A, Dascal N. Regulation of cardiac L-type Ca(2)(+) channel CaV1.2 via the beta-adrenergic-cAMP-protein kinase A pathway: old dogmas, advances, and new uncertainties. Circ Res. 2013;113:617–31. [PubMed: 23948586]
56. Riley G, Syeda F, Kirchhof P, Fabritz L. An introduction to murine models of atrial fibrillation. Frontiers in physiology. 2012;3:296. [PubMed: 22934047]
57. Kirchhof P, Kahr PC, Kaese S, Piccini I, Vokshi I, Scheld HH, et al. PITX2c is expressed in the adult left atrium, and reducing Pitx2c expression promotes atrial fibrillation inducibility and complex changes in gene expression. Circ Cardiovasc Genet. 2011;4:123–33. [PubMed: 21282332]
58. Purohit A, Rokita AG, Guan X, Chen B, Koval OM, Voigt N, et al. Oxidized Ca(2+)/calmodulin-dependent protein kinase II triggers atrial fibrillation. Circulation. 2013;128:1748–57. [PubMed: 24030498]

HIGHLIGHTS

JMCC11927R1: Electrophysiologic and Molecular Mechanisms of a Frameshift NPPA Mutation Linked with Familial Atrial Fibrillation

- The underlying mechanisms by which an *NPPA* mutation causes AF are poorly understood
- We engineered 2 transgenic mouse models expressing the wild-type and humanized *NPPA* mutation
- Mice expressing the *NPPA* mutation were more prone to AF
- This risk was mediated by remodeling of cardiac Na^+, Ca^{2+} and K^+ channels creating a substrate for AF

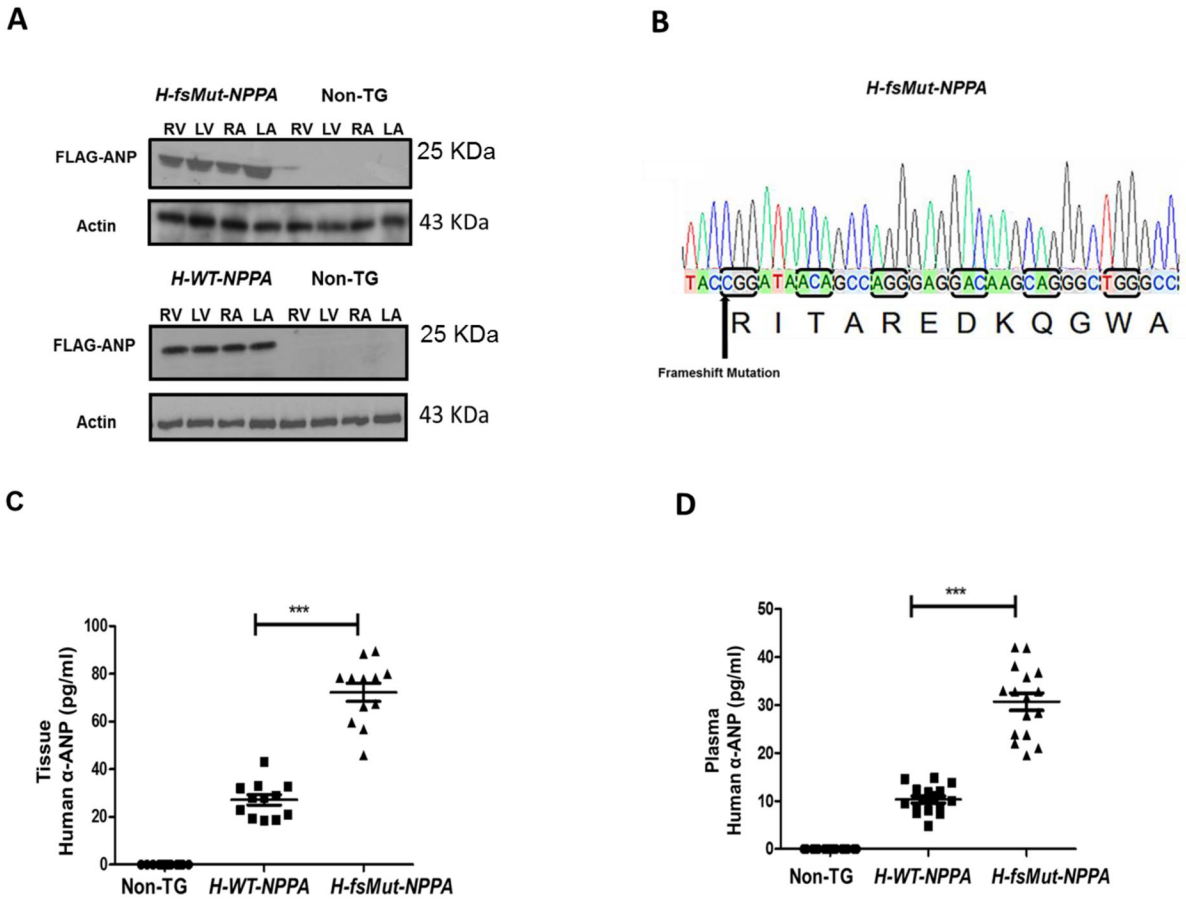

Figure 1: Generation of transgenic (TG) lines expressing human atrial natriuretic peptide (H-ANP):

A: Western Blot analysis of FLAG-tagged H-ANP (wild-type [WT] and mutant [Mut]) in the TG lines *H-WT-NPPA* and *H-fsMut-NPPA* respectively. WT-ANP and Mut-ANP are expressed in all 4 cardiac chambers: right atrium (RA), left atrium (LA), right ventricle (RV), and left ventricle (LV). **B:** Sequencing of H-fsMut-NPPA-Flag PCR fragments confirms the presence of the genetic variant (T>C), double deletion (delAA) and the extension of the 36 base pairs that results in the anomalous 12-residue carboxyl-terminal tail in Mut-ANP (RITAREDKQGWA). **C:** Cardiac tissue concentration of Human α-ANP was measured in the purified protein fraction of heart harvested from the 3 groups of mice using ELISA Kit; n=12/group. **D:** Circulating levels of H-ANP measured in the plasma of the blood collected from the 3 groups of mice using Human-α (1-28 amino acid) ELISA Kit; n=12/group. *H-WT-NPPA* vs *H-fsMut-NPPA*; ***P<0001; data is presented as mean ± SD.

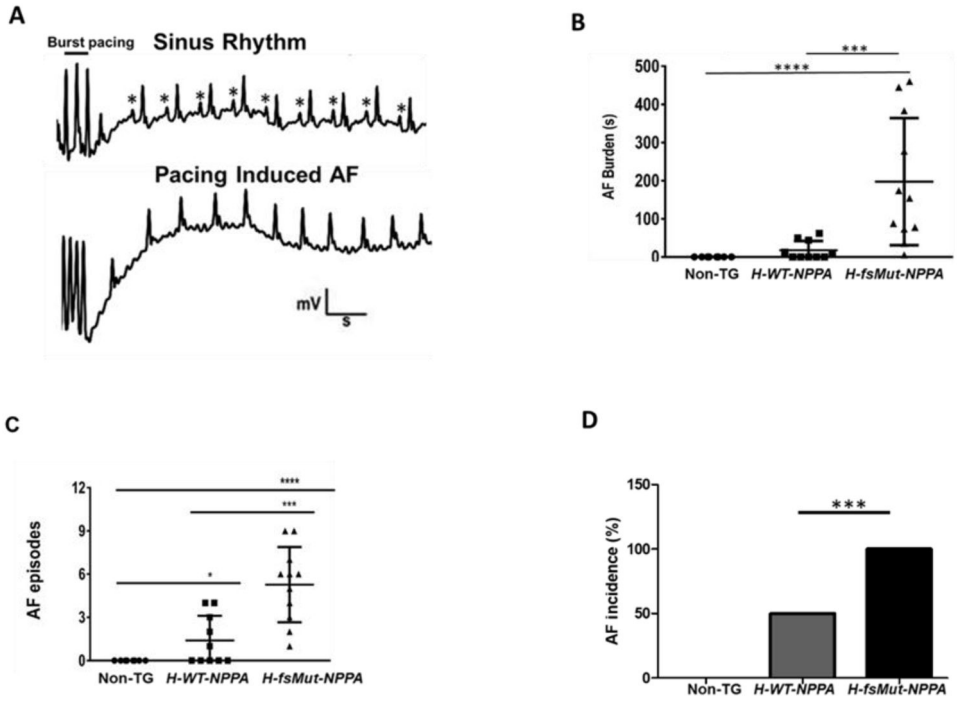

Figure 2: *H-fsMut-NPPA* mice are more prone to pacing-induced atrial fibrillation (AF).
A: Atrial electrograms showing sinus rhythm (*P-wave) at baseline (top) and pacing-induced AF in *H-fsMut-NPPA* mice (bottom). **B:** Burden (duration) of pacing-induced AF in individual mice across the 3 groups; n = 8, 10, and 11 respectively for Non-TG, *H-WT-NPPA*, and *H-fsMut-NPPA* mice. **C:** Number of AF episodes per mouse among the 3 groups. **D**: Incidence of AF among the 3 groups of mice. *P<0.05, **P<0.01; ***P<0.001; ****P<0.0001; data is presented as mean ± SD.

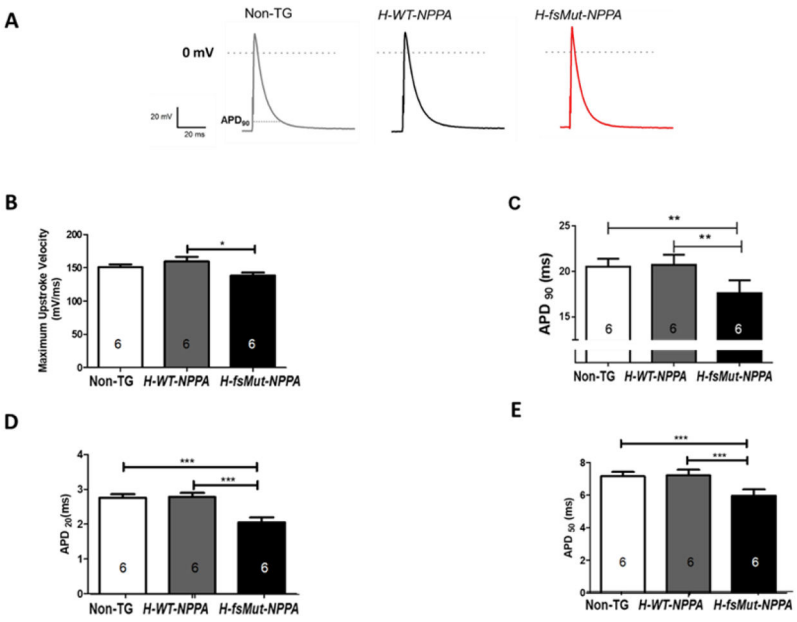

Figure 3: Mut-ANP increases susceptibility to AF by shortening the atrial action potential duration (APD).

A: Schematic representation of atrial AP and electrophysiologic parameters measured in Non-TG, *H-WT-NPPA* and *H-fsMut-NPPA* mice. Measured parameters included: **B:** Maximum upstroke velocity; **C:** APD at 90% repolarization (APD_{90}); and **D-E:** APD at 20% (APD_{20}) and APD at 50% (APD_{50}) repolarization, n=6 mice/group, *P<0.05; **P<0.01; ***P<0.001; data is presented as mean ± SD.

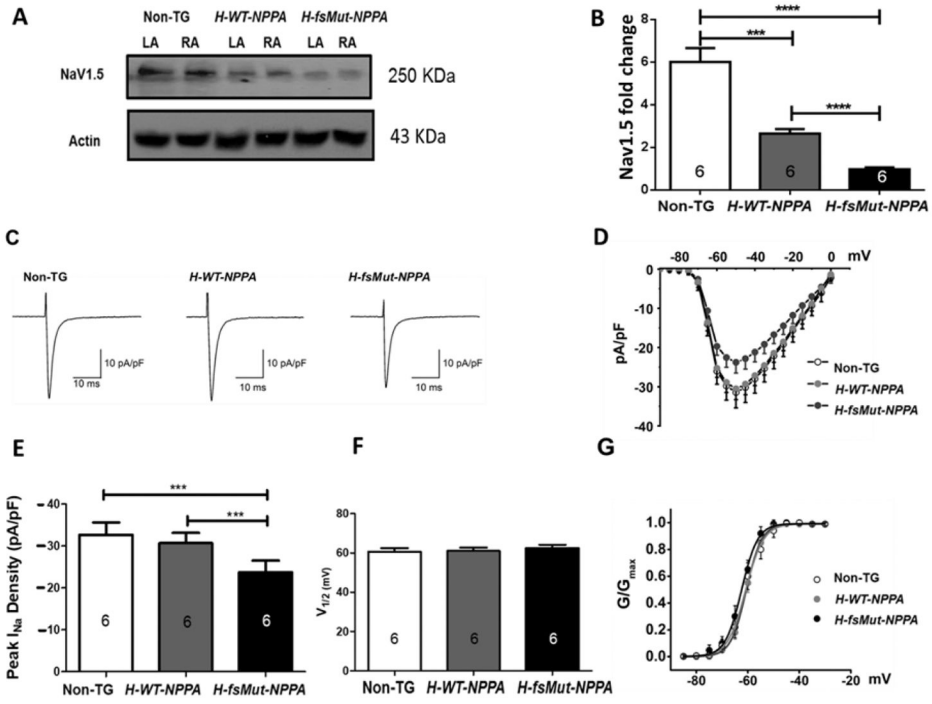

Figure 4: Downregulation of expression of NaV1.5 leads to reduced Na^+ current (I_{Na}) in *H-fsMut-NPPA* mice.

A: Western blot of NaV1.5 expression in Non-TG, *H-WT-NPPA* and *H-fsMut-NPPA* mice, n=6 mice/group. **B:** Fold change in NaV1.5 expression in the 3 groups of mice. **C:** Representative I_{Na} recordings in atrial cells from Non-TG, *H-WT-NPPA* and *H-fsMut-NPPA* mice, n=6 mice/group; currents were activated by depolarization to −50 mV for 50 ms from a holding potential of −100 mV. **D:** Normalized I-V plot of current densities from atrial cells in the 3 groups; statistical analysis of I_{Na} I-V plot shows *** P<0.0001 (Non-TG vs *H-fsMut-NPPA*) as well as (*H-WT-NPPA vs H-fsMut-NPPA*) with 1-way repeated measures ANOVA with Tukey post hoc test; n=6 atrial cardiomyocytes. **E:** Comparison of maximum peak I_{Na} density at −50 mV in the 3 groups of mice. **F:** $V_{1/2}$ (mV) for conductance. **G:** Relative cell conductance normalized for maximal conductance (G/Gmax); curves are Boltzmann fits of the data points. *P<0.05; ***P<0.001; ****P<0.0001; data is presented as mean ± SD.

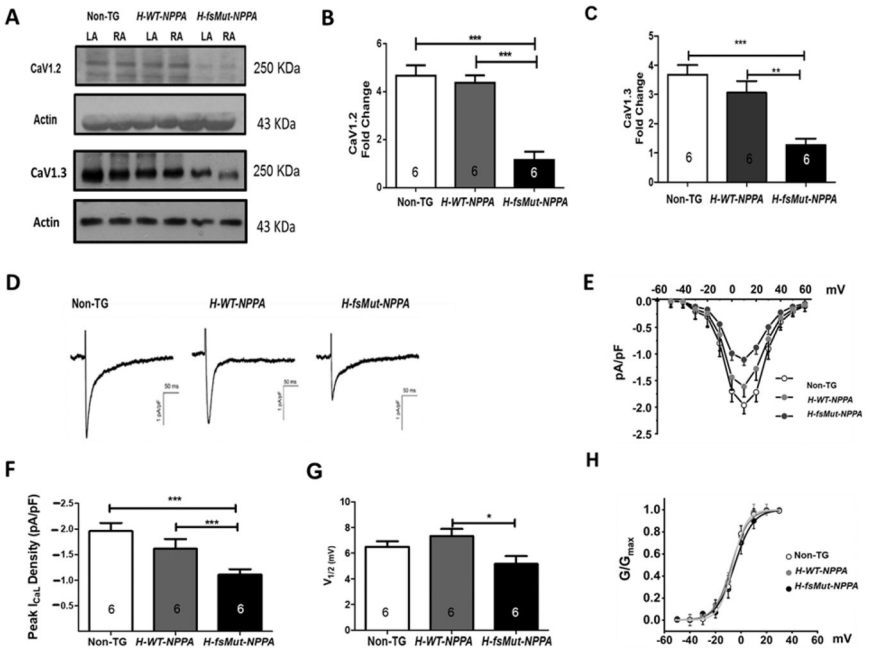

Figure 5: Downregulation of CaV1.2 and CaV1.3 expression leads to reduced L-type Ca current ($I_{Ca,L}$) in *H-fsMut-NPPA* mice.

A: Western blot of CaV1.2 and CaV1.3 expression in Non-TG, *H-WT-NPPA* and *H-fsMut-NPPA* mice, n=6 mice/group. **B-C:** Fold change in CaV1.2 and CaV1.3 expression in the 3 groups of mice. **D:** Representative $I_{Ca,L}$ recordings in atrial cells from Non-TG, *H-WT-NPPA* and *H-fsMut-NPPA* mice; n=6 mice/group. Ca^{2+} currents are activated by depolarization to +10mV from a holding potential of −80mV. **E:** Normalized I-V plot of current densities from atrial cells in the 3 groups of mice. Statistical analysis of $I_{Ca,L}$ IV curve: *** P<0.0001 (Non-TG vs *H-fsMut-NPPA*) and *P<0.05 (*H-WT-NPPA vs H-fsMut-NPPA*) with 1-way repeated measures ANOVA with Tukey post hoc test; n=6 atrial myocytes/group. **F:** Comparison of peak $I_{Ca,L}$ density in the 3 groups of mice. **G:** $V_{1/2}$ (mV) for conductance. **H:** Relative cell conductance normalized for maximal conductance (G/Gmax); curves are Boltzmann fits of the data points. *P<0.05; **P<0.01; ***P<0.001; ****P<0.0001; data is presented as mean ± SD.

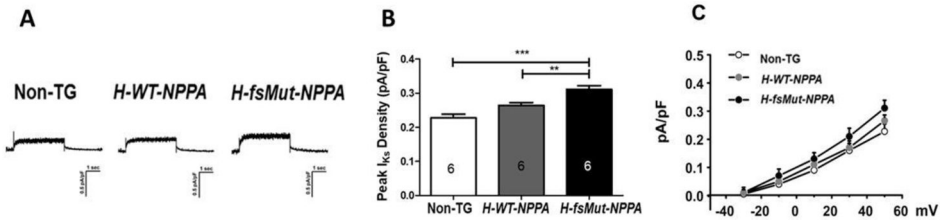

Figure 6: Increased I_{Ks} density:

A Representative I_{Ks} recordings in atrial cells from Non-TG, *H-WT-NPPA* and *H-fsMut-NPPA* mice, n=6 mice/group. I_{Ks} were elicited by using 4 s voltage-clamp steps to test potentials of −30 to +50 mV, with 20 mV increments. **B** Comparison of peak I_{Ks} density in the 3 groups of mice. **P<0.01; ****P<0.0001; data is presented as mean ± SD. **C** Normalized I-V plot of current densities from atrial cells in the 3 groups of mice. Statistical analysis of I_{Ks} IV curve: **P<0.01 (Non-TG vs *H-fsMut-NPPA*), and *P<0.05 (*H-WT-NPPA vs H-fsMut-NPPA*), with 1-way repeated measures ANOVA with Tukey post hoc test; n=6 atrial myocytes/group.

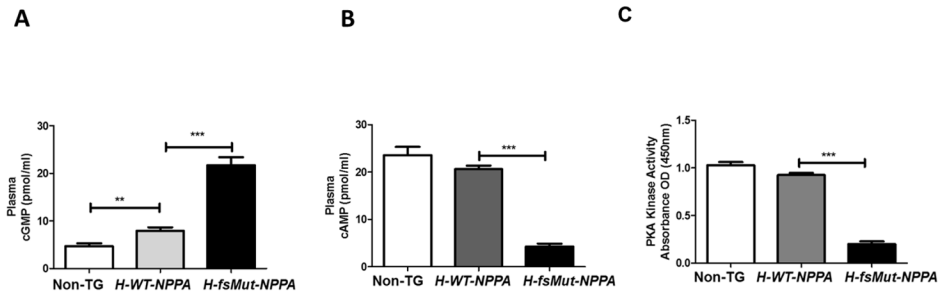

Figure 7: Mut-ANP modulates cardiac ion channels by activating cGMP-cAMP-PKA signaling pathway.

Baseline plasma cGMP levels were measured in Non-TG, *H-WT-NPPA* and *H-fsMut-NPPA* using an in-vitro cGMP EIA kit. **A:** Plasma cGMP levels were higher in *H-fsMut-NPPA* mice versus *H-WT-NPPA* and Non-TG mice. **B:** cAMP levels were reduced in *H-fsMut-NPPA* mice when compared to *H-WT-NPPA* and Non-TG mice. **C:** PKA activity was reduced in the atrial tissue of *H-fsMut-NPPA* mice when compared to *H-WT-NPPA* and Non-TG mice. n=12/group; **P<0.01 and ***P<0.0001; data is presented as mean ± SD. cAMP, cyclic adenosine monophosphate; cGMP, cyclic guanosine monophosphate; PKA, protein kinase A.

Table 1:

Mean arterial pressure (MAP) in the 3 groups of mice at baseline and post-infusion of synthetic fs-Mut-ANP and WT-ANP.

STRAIN	MAP (mmHg)	30 min post fs-mutant ANP	120 min post fs-mutant ANP	P-value (MAP pre ANP vs 30 min post ANP treatment
Non-TG	121 ± 2	107 ± 3	125 ± 2	<0.0001
H-WT-NPPA	102 ± 3	80 ± 2	99 ± 5	<0.0001
H-fsMut-NPPA	76 ± 4	52 ± 3	71 ± 4	0.0009

STRAIN	MAP (mmHg)	30 min post Wildtype ANP	120 min post Wildtype ANP	P-value (MAP pre ANP vs 30 min post ANP treatment
Non-TG	127 ± 4	121 ± 3	131 ± 4	ns
H-WT-NPPA	106 ± 3	101 ± 4	104 ± 6	ns
H-fsMut-NPPA	72 ± 6	69 ± 5	74 ± 3	ns

H-fsMut-NPPA, humanized frameshift natriuretic precursor peptide A; *H-WT-NPPA*, humanized wild-type *NPPA*; ns, non-significant; TG, transgenic. n=12 mice/group; data is presented as mean ± SD.

Table 2:

Electrocardiographic (ECG) characterization of the 3 groups of mice.

Strain	PR interval (msec)	QT interval (msec)	QRS duration (msec)
Non-TG	39.8 ± 3.7	68.3 ± 2.9	22.3 ± 1.6
H-WT-NPPA	41.5 ± 2.6	73.8 ± 1.9	28.3 ± 2.1
H-fsMut-NPPA	47.2 ± 3.2	81.2 ± 3.1	38.6 ± 3.1*

ECG parameters measured in the 3 groups of mice, n=12 mice/group. QRS duration in *H-fsMut-NPPA* mice (*) was significantly prolonged versus *H-WT-NPPA* mice ($P<0.05$) and Non-TG mice ($P<0.001$). Other abbreviations as in Table 1.